## Proceedings of the Institute of Acoustics

Performance of Horizontal Towed Arrays

Effect of Internal Waves

B.J. Uscinski

Ocean Acoustics Group, Department of Applied Mathematics and Theoretical Physics, University of Cambridge, Silver Street, Cambridge CB3 9EW, U.K.

#### 1. INTRODUCTION

Horizontal towed arrays are used to detect faint or distant acoustic sources in the ocean. These arrays are sometimes very long since angular resolution increases with array length and more acoustic energy is collected. There are, however, limits beyond which the array length cannot be usefully increased. The presence of saturated internal wave fields in most oceans provides one such limit since these waves restrict the spatial coherence of acoustic signals and introduce and intrinsic ambiguity in the direction of arrival. Increasing array resolution beyond this limit is meaningless and this restricts useful array length. It also implies that there is an optimum array length.

Similar questions arise as to whether there is an optimum frequency at which to operate an array of a given length. Again the presence of internal waves imposes limitations. The higher the acoustic frequency the narrower the beam pattern, but the amount of scattering increases with frequency and this eventually destroys array resolution. This paper investigates these questions by using the Garrett-Munk model of ocean internal waves to derive simplified expressions for coherence of the acoustic field and array response in these conditions. Estimates are obtained for the optimum array length and operating frequency in various propagation regimes. Finally the effect of towing speed is considered, and it is shown that an additional effect due to the time variation of the internal wave field can be important if the array is towed very slowly.

## 2.THE EFFECT OF INTERNAL WAVES ON ACOUSTIC COHERENCE

Long acoustic arrays are used for much the same reasons as are large mirrors or lenses in telescopes. The layer aperture increases angular resolution and gathers more light. However, the large telescope can only be used to good effect on the top of mountains where the air is rarefied, or better still, out in space where there is no atmosphere. Atmospheric turbulence bends light rays in a random manner, destroying the coherence of a wave-front and impairing the resolving power of the lens or mirror. In the same way the oceans contain many types of turbulence and waves that destroy the coherence of

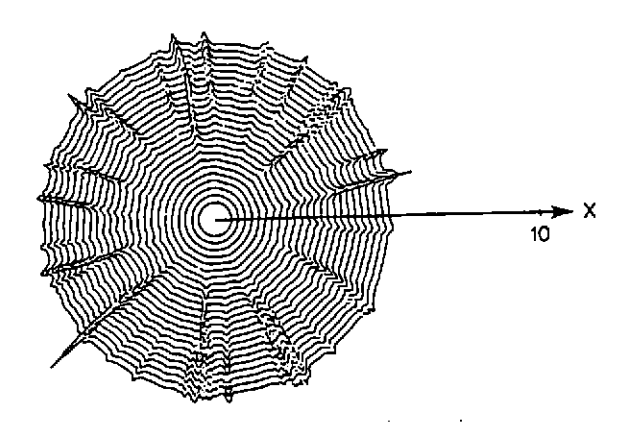


Fig. 1. Numerical simulation of an acoustic wave propagating from a point source through a homogeneous isotropic random medium. The innermost circle denotes the scale size of an average irregularity.

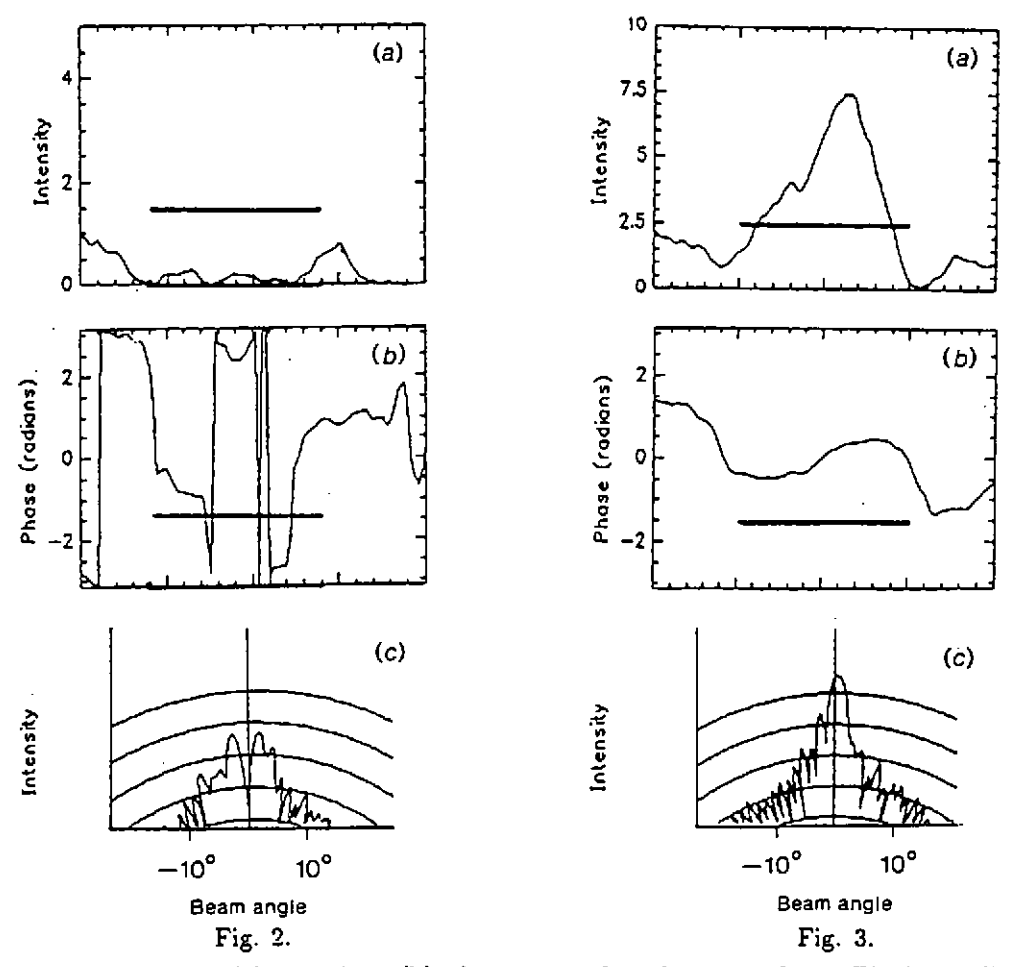


Fig. 2. Intensity (a) and phase (b) of a section of random wave-front. The heavy line gives the position of the array. The corresponding intensity response of the array as a function of angle is also shown in (c).

Fig. 3. The same as in Fig. 2. but over a different section of the wave-front.

an acoustic wave front. However, the acoustic array, unlike the telescope, must always be immersed in this fluctuating medium and must suffer the consequences.

Let us consider the physical characteristics of an incoherent field. This is illustrated most easily by looking at the intensity pattern of a point source situated in a medium containing random structures. Figure 1 shows a particular case calculated by numerical simulation [1]. At each radial range the departure of the line from a circle is proportional to the intensity. We see that the irregular medium introduces peaks and troughs of intensity in the sound wave. These can be quite large and the accompanying variations of phase can be large also. These will clearly have a marked effect on the output of an acoustic array receiving such a field. We look at two particular cases.

Figure 2 shows the amplitude and phase of a small region of the acoustic wavefront over the array. The corresponding intensity beam pattern of the array is also shown and exhibits a double or split main lobe which can be linked to the v-shaped phase variation over the array. In this case the equivalent source would be a double source with a few degrees separation.

A different region of the wavefront is shown in Figure 3. Here the intensity is much greater and the phase variation is smooth. The beam pattern has a very strong single main lobe with direction slightly displaced to the left, again due to the phase variation over the array.

We see that the irregular wavefront has two main effects on the array response:

- (a) The phase structure in front can displace the beam pattern or even split it, leading to an uncertainty in the position of the source.
- (b) The intensity peaks and troughs can result in a very strong or very weak response, for example the main lobe maximum in Figure 2 is 2 is about a hundred times weaker than that in Figure 3. Thus the irregular intensity can mean that a source could go undetected.

## 2.1 Coherence Length

The random phase and amplitude features in the wave field are sometimes characterised by a quantity called the "coherence length", which is the average size of these features. In what follows we examine how changing the array length relative to the field coherence length can affect array performance in the case where the randomness in the medium is caused by internal waves and the array is horizontal.

#### 3.ARRAY RESPONSE IN SATURATION INTERNAL WAVE FIELD

An acoustic source of wave number k is at the origin of a Cartesian set of axes x, y, z, with z directed downwards, in an ocean containing a saturated internal wave field whose

vertical and horizontal scales are  $L_V$  and  $L_H$  respectively. Let

$$Z = z/L_V , Y = y/L_H , X = x/kL_V^2 .$$
 (1)

The array of length  $L_a$  having closely and equally spaced hydrophones lies in the y direction, intersected at midpoint by the x axis at a scaled range X from the origin, and has a scaled length  $\ell_a = L_a/L_H$ .

The ensemble average power output of the array for a plane-wave component of acoustic energy arriving from a direction making an angle  $\theta$  with the x axis is in this case [2], [3]

$$I(\theta, Z, X) = 2 \int_0^{\ell_a} (\ell_a - \bar{\eta}) m_2(0, \bar{\eta}, X) \cos\{\nu_1 \bar{\eta}\} d\bar{\eta} , \qquad (2)$$

where  $m_2(\bar{\zeta}, \bar{\eta}, X)$  is the second moment of the acoustic field, and

$$\bar{\zeta} = Z_1 - Z_2 ,$$

$$\bar{\eta} = Y_1 - Y_2 ,$$

$$\nu_1 = k L_H \sin \theta .$$
(3)

Thus  $I(\theta, Z, X)$  is the average angular intensity response pattern of a linear array to acoustic energy that has passed through a saturated internal wave field. In the case of a point source

$$m_2(\bar{\zeta}, \bar{\eta}, X) = \exp\left\{-\Gamma X \int_0^1 [1 - f_0(\bar{\zeta}t, \bar{\eta}t)]dt\right\} , \qquad (4)$$

where  $\Gamma$  is the scattering strength parameter of the medium  $\Gamma$  is the scattering strength parameter of the medium

 $\Gamma = k^3 \mu^2 L_H L_V^2 , \qquad (5)$ 

 $\mu^2$  is the mean square value of fractional sound speed variations with autocorrelation function  $\rho(\bar{\zeta}, \bar{\eta}, \bar{\xi})$ , and

$$f(\bar{\zeta}, \bar{\eta}) = \int_{-\infty}^{\infty} \rho(\bar{\zeta}, \bar{\eta}, \bar{\xi}) d\bar{\xi} ,$$
  

$$f_0(\bar{\zeta}, \bar{\eta}) = f(\bar{\zeta}, \bar{\eta}) / f(0, 0) .$$
(6)

## 3.1 Internal Waves

The quantity  $f_0$  can be calculated for a saturated internal wave field whose normalised spectrum of vertical spatial frequencies  $\beta$  is given by [4]

$$H(\beta) = \left[\pi - 2\operatorname{arct}g(1/j_{\bullet})\right]^{-1} \frac{\beta_{\bullet}}{(\beta_{\bullet}^{2} + \beta^{2})} \qquad (\beta > \beta_{0})$$

$$= 0 \qquad (\beta < \beta_{0}) \qquad (7)$$

where

$$\beta_{\bullet} = L_V^{-1} , \qquad (8)$$

is the turn-over spatial frequency and  $\beta_0$  is the lower cut-off spatial frequency

$$j_* = \beta_*/\beta_0 \ . \tag{9}$$

The coherence  $m_2$  in (4) involves the integrated form of  $f_0$ 

$$F(\bar{\eta},0) = \int_0^1 f_0(\bar{\eta}t,0)dt \ . \tag{10}$$

In the case of the spectrum (7) this becomes [3,4]

$$F(\bar{\eta},0) = \frac{4}{\bar{\eta} \ln(1+j_*^2)} \int_{1/j_*}^{\infty} \left[ \int_0^{\infty} \frac{\sin(xy\bar{\eta})}{(1+y^2)^2} dy \right] \frac{dx}{(1+x^2)x^2} , \qquad (11)$$

which is shown in Figure 4 for  $j_* = 3, 5, 7$  by the full line.

A number of useful analytical approximations can be made to simplify (11). A good fit is given by the exponential

$$F(\bar{\eta}, 0) \sim \exp\{-|\bar{\eta}/\bar{\eta}_0|\}$$
 (12)

where

$$\bar{\eta}_0 = 1 + 0.8j_* \ . \tag{13}$$

The approximate form is shown in Figure 4 by the broken line. The agreement is quite adequate for all practical, and indeed most theoretical purposes. The approximation has been checked for values of  $j_* \leq 10$ .

¿From (2) and (12) the average directional pattern of the array is

$$I(\theta, Z, X) = 2 \int_0^{\ell_a} (\ell_a - \bar{\eta}) \exp\{-\Gamma X (1 - e^{-\bar{\eta}/\bar{\eta}_0})\} \cos(\nu_1 \bar{\eta}) d\bar{\eta} . \tag{14}$$

which is the Fourier transform of the product of two functions [3]. The first of these is the autocorrelation function of the array, a triangle of half-base  $\ell_a$ . The second is the horizontal coherence of the acoustic field. When  $\Gamma X \geqslant 2$  this latter becomes, with a good degree of approximation,  $\exp\{-\Gamma X \bar{\eta}/\bar{\eta}_0\}$ .

In all the subsequent numerical calculations we shall take  $j_* = 3$ , which is a representative value for many parts of the ocean.

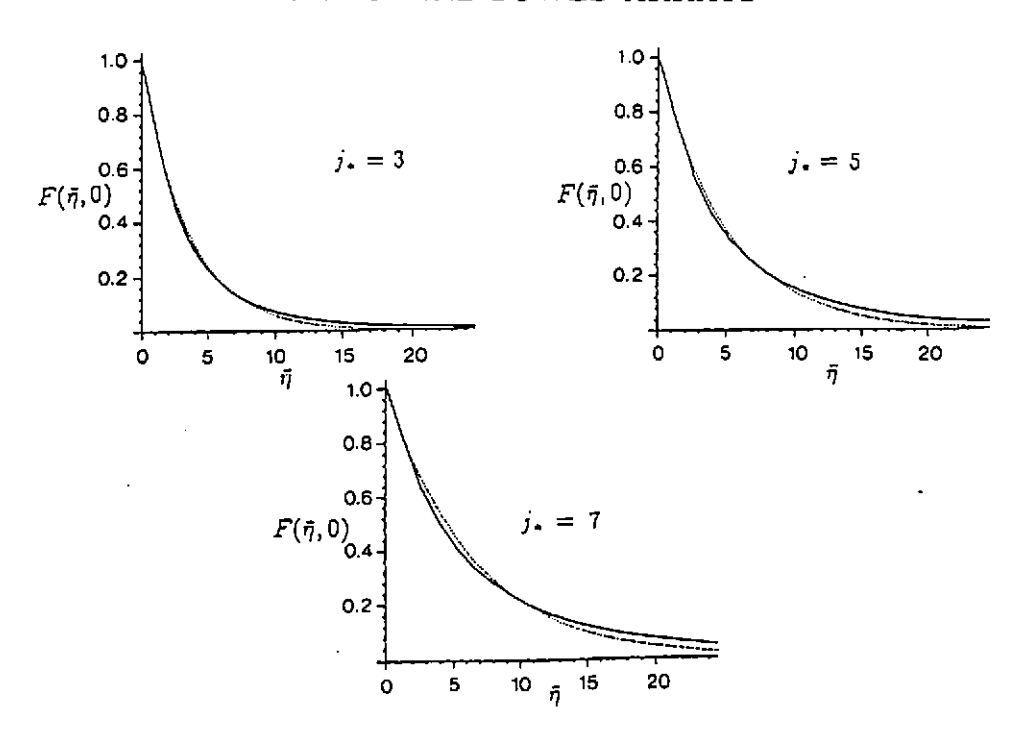


Fig. 4. The projected and integrated horizontal and autocorrelation function of internal waves  $F(\bar{\eta}, 0)$ , (11). The broken line is the exponential approximation (12).

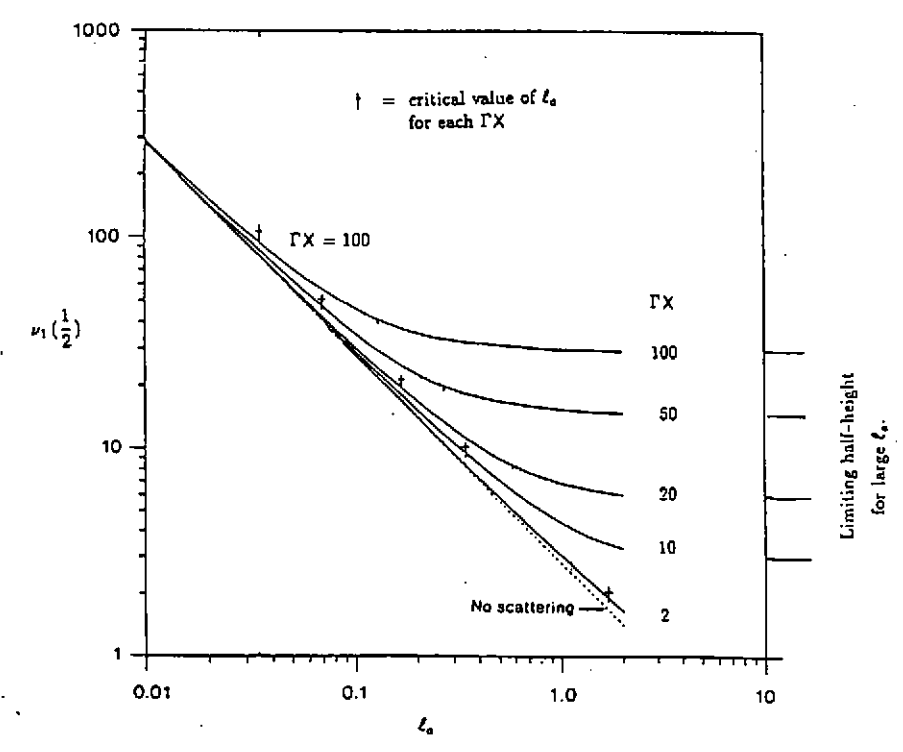


Fig. 5. Angular width of the beam at half-height as a function of array length for various amounts of scattering  $\Gamma X$ .

## 4.THE OPTIMUM ARRAY LENGTH

There are two criteria that can be used to determine how long an array can be made while still gaining a worthwhile advantage. These are the angular resolution of the array and its intensity response. We now use the results of the previous section to examine each of these criteria.

#### 4.1 Angular Resolution

When the field coherence is very much wider than the array autocorrelation  $\ell_a$  the array pattern I is given by the Fourier transform of this autocorrelation and thus has a main lobe whose width is

$$\theta_a \approx \lambda/2L_a \ . \tag{15}$$

As the medium has more effect and the field coherence becomes narrower I is given by the Fourier transform of the coherence and its width increases. In this case

$$I(\theta, Z, X) \approx I_0[1 + (\theta/\theta_s)^2]^{-1}$$
, (16)

with

$$I_0 = 2(1 + 0.8j_*)/\Gamma X$$
,,  
 $\theta_s = k\mu^2 x/(1 + 0.8j_*)$ .. (17)

If the scattering by internal waves is not to have a marked effect on the width of I it can be seen from the above that we require

$$L_a \lesssim L_a(\text{crit}) = (1 + 0.8j_*)/k^2\mu^2 x$$
 (18)

or

$$l_a(\text{crit}) = (1 + 0.8j_*)/\Gamma X$$
 (19)

This can be regarded as a critical array length. Extending the array beyond this limit will not lead to any improvement of directivity.

Some more insight into the effect of the medium can be gained by considering curves of the main lobe width as a function of array length calculated from (14). Let  $\nu_1(1/2)$  be the value of  $\nu_1$ , (3), at the -3dB level (i.e. the beam width at half height). Figure 5 shows  $\nu_1(1/2)$  as a function of the scaled array length  $l_a$  for various values of  $\Gamma X$ , i.e. for different amounts of scattering by the medium. The broken line is the case  $\Gamma X = 0$ , i.e. no internal waves. In this case the beam width decreases in inverse proportion to the array length, as would be expected. When  $\Gamma X$  is non-zero the beam width decreases with an increase in  $l_a$  only to a certain width which we shall call  $\nu_1(1/2,\infty)$ , i.e. the angular width as  $l_a$  approaches infinity. This limiting value of  $\nu_1(1/2)$  is determined by the scattering. The larger  $\Gamma X$  the larger is  $\nu_1(1/2,\infty)$ .

It is also clear from the curves of Figure 5 that there is a certain array length beyond which little narrowing of the beam occurs and  $\nu_1(1/2)$  is close to its limiting value  $\nu_1(1/2,\infty)$ . The values of  $l_a(\text{crit})$  estimated above, (19), are marked on the curves of Figure 5 with crosses. There may be a case for taking  $l_a(\text{crit})$  to have a larger value in order for  $\nu_1(1/2)$  to be closer to its limiting value.  $\nu_1(1/2,\infty)$ , which can be shown from (14) to be

$$\nu_1(1/2, \infty) = \Gamma X / (1 + 0.8j_*) . \tag{20}$$

These limiting values are also marked on the right hand vertical axis of Figure 5 and agree well with the computed curves.

#### 4.2 Intensity Response

Making the array longer not only produces a narrower beam but also increases the amount of energy collected by the array. We now ask what is the optimum array length as judged by this criterion. While a longer array collects more signal the amount of ambient noise received also increases, but it is reasoned that the noise, being omnidirectional, is spatially incoherent and so N components of noise amplitude  $A_N$  add incoherently to give a noise intensity

$$I_N = \Sigma_N A_N^2 = N A_N^2 . (21)$$

The signal, on the other hand, is assumed to be unidirectional and so its N components of amplitude  $A_S$  add coherently to give a signal intensity

$$I_S = (\Sigma_N A_S)^2 = N^2 A_S^2 . (22)$$

Thus the intensity of the received signal should grow like the square of the number of components, i.e. as the square of the array length, while the noise should grow in proportion to the array length only. Consequently, a longer array should be able to detect weaker signals since it has a larger signal to noise ratio than a shorter array.

The effect of internal waves on the acoustic signal is such that this gain can be appreciably reduced. The internal waves distort the signal wave-front so that it is no longer unidirectional, but arrives from a range of angular directions and is to some extent like the omnidirectional noise. The signal strength no longer increases like the square of the array length and the expected signal to noise ratio is reduced.

In order to study this effect we return to expression (14) and consider its behaviour at the centre of the main lobe,  $\langle I(0,Z,R) \rangle = I(0)$ , i.e.  $\nu_1$  equal to zero. As before  $j_* = 3$  and the result I(0), as a function of array length  $l_a$ , depends only on  $\Gamma X$ . These curves are shown in Figure 6. The curve for  $\Gamma X = 0$  represents the case when there is no scattering of the signal by the medium and I(0) grows like the square of  $l_a$ .

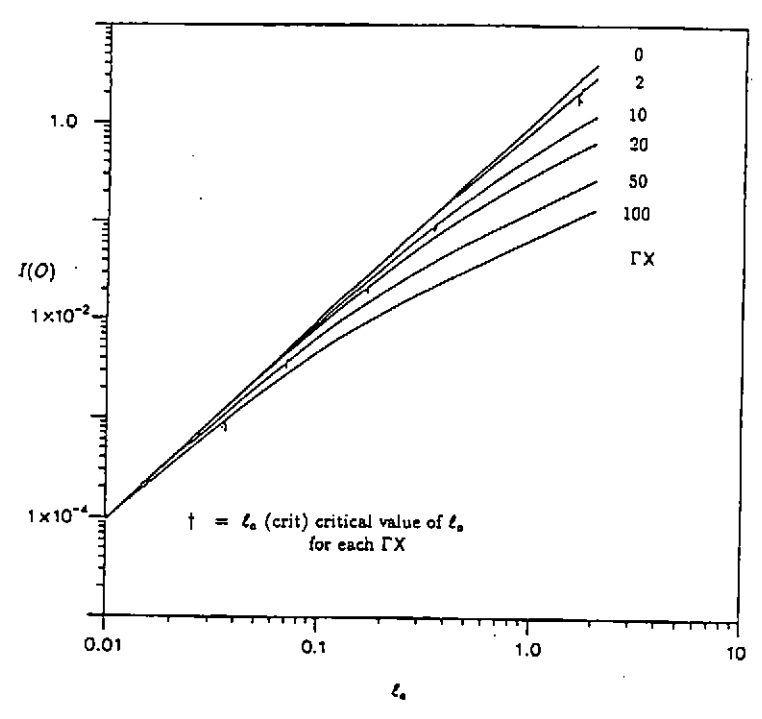


Fig. 6. Relative intensity at centre of the beam pattern as a function of array length for various amounts of scattering  $\Gamma X$ .

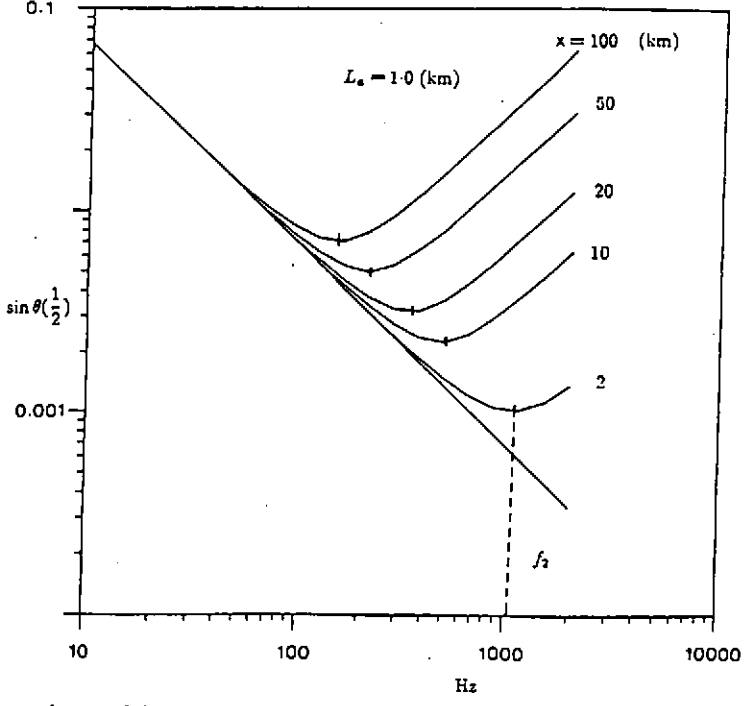


Fig. 7. Angular width of beam at half-height as a function of acoustic frequency for an array of length 1 km. shown for different ranges of propagation.

The other curves of I(0) are shown relative to the  $\Gamma X = 0$  signal since we do not have an absolute measure of the signal strength (although this could be given if the range and source level were known). We see that for non-zero values of  $\Gamma X$  the strength I(0) ceases to rise like the square of the array length, and as  $l_a$  increases I(0) grows in proportion to  $l_a$ , like the result predicted for noise. Thus internal waves and the distortion they introduce into the signal mean that increasing the array length beyond a certain critical length of  $l_a$  does not result in the expected gain in signal to noise ratio. This is similar to the result described in the previous section on the beam width.

#### 4.3 A Simple Analytical Model

A simple analytical model can now be used to provide some measure of check on these estimates. We make the approximation for large  $\Gamma X$ , discussed in Section 3 so that (14) becomes

$$\langle I(\theta, X) \rangle = 2 \int_0^{\ell_a} (\ell_a - \bar{\eta}) e^{-A\bar{\eta}} d\bar{\eta} , \qquad (23)$$

where

$$\begin{array}{rcl}
A & = & \left[\Gamma X/\bar{\eta}_0 - i\nu_1\right] \\
\nu_1 & = & kL_H \sin\theta
\end{array} \right\} .$$
(24)

The integral in (23) can be carried out analytically to give

$$\langle I(\theta, X) \rangle = \frac{2}{(a^2 + \nu_1^2)^2} \left\{ (a^2 - \nu_1^2)(a\ell_a - 1) + 2a\nu_1^2 \ell_a + e^{-a\ell_a} [(a^2 - \nu_1^2)\cos(\nu_1 \ell_a) - 2a\nu\sin(\nu_1 \ell_a)] \right\},$$
(25)

where

$$a = \Gamma X/\bar{\eta}_0 \ . \tag{26}$$

A further simplification is possible if  $\Gamma X$  is appreciably greater than unity. In this case, since  $\ell_a$  is of order unity, the exponential term in (2.5) becomes extremely small. Moreover, a is large by virtue of  $\Gamma X$  and so, to a good degree of approximation

$$\langle I(\theta, X) \rangle = \frac{2a^3 \ell_a}{(a^2 + \nu_1^2)^2}$$

$$\langle I(0, X) \rangle = \frac{2\ell_a}{a}$$
(27)

The above calculations assume that there is an appreciable amount of scattering by internal waves. In the absence of scattering  $\Gamma=0$  and (23) is easily integrated, showing that for  $\theta=0$ 

138

$$\langle I(0,X)\rangle = \ell_a^2 \ . \tag{28}$$

The transition point between the square law and linear dependence on  $\ell_a$  gives an estimate of  $\ell_a$  (crit) and is, from (27) and (28)

$$\ell_a(\text{crit}) = 2\eta_0/\Gamma X$$

$$= 2(1 + 0.8j_*)/\Gamma X . \tag{29}$$

The crosses on the curves of Figure 6 show the same  $l_a$  (crit) as that calculated for Figure 5 and given by (19). Clearly, this estimate of  $l_a$  (crit) could be altered by imposing a different requirement on the closeness with which we wish to approach the limiting value of either angular resolution (in the case of Figure 5) or of array gain (Figure 6). Referring to Figure 5 we see that by taking a new criterion for  $l_a$  (crit) such that

$$l_a(\text{crit}) = 2(1 + 0.8j_{\bullet})/\Gamma X \tag{30}$$

the angular width at half-height  $\nu_1(1/2)$  is reduced by a factor of about two. This might well be a better point to place the position of  $l_a$  (crit) since, although the inverse linear relationship between array length and beam width is now beginning to fail (a two-fold improvement in resolution for a two-fold increase in length), there is still an appreciable pay-off to be had. Further increasing to give a new limit  $l'_a$  (crit) equal to  $3l_a$  (crit) leads to an improvement in beam width by a factor of only 1.4 and so the relative pay-off is now much less attractive.

The most interesting aspect of the above calculations is that the optimum array length turns out to be approximately the same, whether calculated on the basis of narrowest beam or maximum intensity it is of the order

$$L_{a_{(opt)}} = \bar{\eta}_0 c^2 / 4\mu^2 \pi f^2 x . \tag{31}$$

For the depth used in the present example and a standard internal wave field this can be specified to

$$L_{a_{(opt)}}(m) = 108 \times 10^4 (\lambda^2/x)(m)$$
 (32)

Note that the result (3.2) is at odds with the some-times quoted (without any clear justification) statement that the best array length is equal to 128  $\lambda$ .

## 5. THE OPTIMUM ACOUSTIC FREQUENCY

Sometimes it may be necessary to pose the question about array performance in a different way. For example, the array might be used in an active mode to transmit as in a Low Frequency Active Sonar (L.F.A.S.). In this case it may be necessary to decide what is the best operating frequency for an array of a given length. As a criterion we can require that the beam width at half-height be a minimum. To illustrate the problem equation (14) is used to plot the half-height value  $\sin \theta(1/2)$  as a function of

acoustic frequency for an array of fixed length equal to 1 km. This is shown in Figure 7 for various distances from a point source assuming a standard internal wave field.

Each curve behaves in the same way. As the frequency increases the wavelength decreases and the angular aperture becomes narrower. As the frequency increases further the medium scatters more and the beam width is dominated by the scattering angle leading to a wider beam. The optimum frequency occurs at the minimum and can be determined as follows:

The angular response of the array, normalised to unity for  $\theta = 0$ , can be written as

$$I_0(\theta, X) = \langle I(\theta, X) \rangle / \langle I(0, X) \rangle$$
  
=  $(1 + (\sin^2 \theta / \sin^2 \theta_0))^{-2}$ , (33)

where

$$\sin \theta_0 = \frac{k\mu^2 x}{\bar{\eta}_0} \ . \tag{34}$$

Now the amplitude is at half-height when  $\sin \theta = \sin \theta_0$  and so the width of the array pattern at half-height is

$$\sin \theta(\frac{1}{2}) = k^2 \mu^2 x / \bar{\eta}_0 \ . \tag{35}$$

This expression holds for  $\Gamma X$  large, i.e. for k large, since

$$\Gamma X = k^2 \mu^2 L_H x , \qquad (36)$$

and it corresponds to the rising part of the curves in Figure 7.

In the case of k small  $\Gamma X \ll 1$ , and

$$A = i\nu_1 . (37)$$

Thus

$$\langle I(\theta, X) \rangle = \ell_a^2 [\sin(\nu_2 \ell_a/2) / (\nu_2 \ell_a/2)] , \qquad (38)$$

which is the array pattern for very low acoustic frequencies when the effect of the medium vanishes. The main lobe width is given by

$$\nu_1 \ell_a / 2 = \pi / 2 \ , \tag{39}$$

which gives

$$\sin\theta(\frac{1}{2}) = \pi/kL_a \ . \tag{40}$$

This corresponds to the falling part of the curve in Figure 7. The narrowest array pattern is given by the k for which the two curves intersect. Equating (35) and (40) we have

$$k_{opt} = (\pi \bar{\eta}_0 / L_a \mu^2 x)^{\frac{1}{2}} \tag{41}$$

and

$$f_{opt} = k_{opt}c/2\pi . (42)$$

This expression can be evaluated for the parameters corresponding to the curves in Figure 7 and compared with the computed results. The two are in good agreement, indicating that this simple model is both accurate and very useful.

## 5.1 Relation to Optimum Length

We conclude by showing that optimization by length on acoustic frequency leads to almost the same result. For an array of the critical length given by (30) the corresponding frequency, denoted by f(crit), is related to the  $f_{opt}$  of (42) by

$$f_{(opt)} = \left(\frac{\pi}{2}\right)^{1/2} f(\text{crit})$$

$$= 1.25 f(\text{crit}) . \tag{43}$$

## 6. TIME VARIATION AND ARRAY PERFORMANCE

So far we have been concerned with the spatial effects of an internal wave field on the acoustic signal received by a long towed array, effects such as degradation of the angular resolving ability and gain. However, internal waves in the ocean vary with time and now we wish to examine time variation of some of the characteristics considered in the previous sections. This is particularly relevant if the array is stationary or moving very slowly. We need to know the time periods over which we expect the signal to fluctuate or "fade".

#### 6.1 The quantity $F(\bar{\eta}, \bar{\tau})$

The basic result, (2) and (4), shows that the angular dependence of array intensity depends on the internal wave field through the projected and integrated autocorrelation F. If the time dependence of the internal wave field is retained and the standard Garrett-Munk form [4] of the spectrum is used an expression for  $F(\bar{\eta}, \bar{\tau})$  can be derived. Details of the derivation are not given here but the final result is

$$F(\bar{\eta}, \bar{\tau}) = \frac{4}{\ln(1+j_*^2)} \int_{1/j_*}^{\infty} \frac{1}{(1+x^2)x^2} \int_{0}^{\infty} \sin(xy\bar{\eta}) \cos(\bar{\tau}\sqrt{(1+y^2)/(1+a^2y^2)}) [\bar{\eta}(1+y^2)^2]^{-1} dxdy ,$$
(44)

## Proceedings of the Institute of Acoustics

#### PERFORMANCE OF HORIZONTAL TOWED ARRAYS

where

$$\bar{\tau} = (t_1 - t_2)/T_i \tag{45}$$

is the time lag scaled by

$$T_i = f_i^{-1} (46)$$

a time  $T_i$  equal to the inverse of  $f_i$ , the inertial frequency. At mid-latitudes  $f_i \approx 1.7 \times 10^{-5}$  hours which means that  $T_i$ , the scale on which the internal wave field changes is of the order of 20 hours. The other symbols have the same meaning as before.

The behaviour of  $F(\bar{\eta}, \bar{\tau})$  is shown in Figures 8, 9. In what follows we take

$$i_* = 3$$
,  $a = f_i/n = 1/20$ .

Figure 8 shows  $F(\bar{\eta}, \bar{\tau})$  as a three-dimensional representation while Figure 9 gives the same as a contour diagram.

#### 6.2 Slowly moving receiver

We are now able to consider how radically motion of a receiver will affect the received signal. A receiver moving with a velocity v will cover a distance

$$x = vt \tag{47}$$

in time t. Thus

$$(x_1 - x_2) = V(t_1 - t_2) . (48)$$

Using  $L_H$  and  $T_i$  to scale space and time separations as before, we have

$$\bar{\eta} = V\bar{\tau} \tag{49}$$

as the line corresponding to the receiver motion, where

$$V = vt_i/L_H . (50)$$

Example

Take

$$v = 9 \text{km/hr}$$

$$L_H = 3 \text{km}$$

$$T_i = 20 \text{hr}$$
(51)

Then

$$V \approx 60$$
.

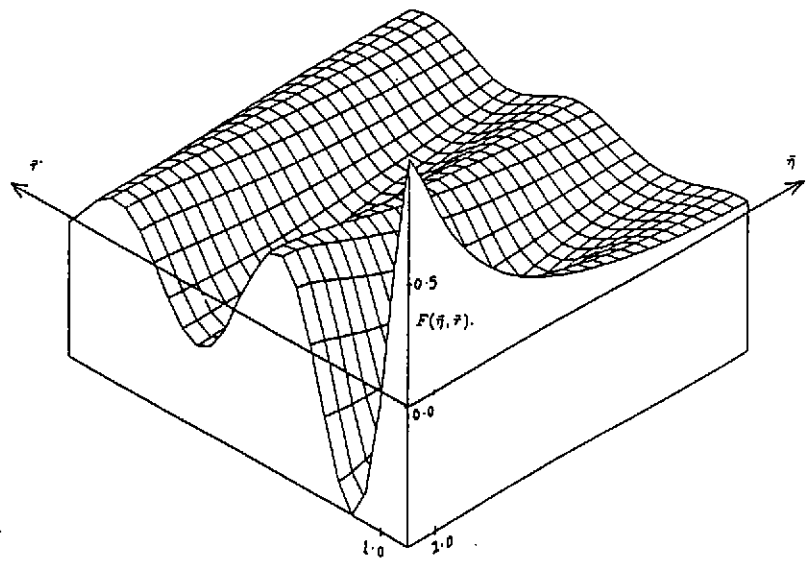


Fig. 8. The time space autocorrelation function  $F(\bar{\eta}, \bar{\tau})$ , (44).

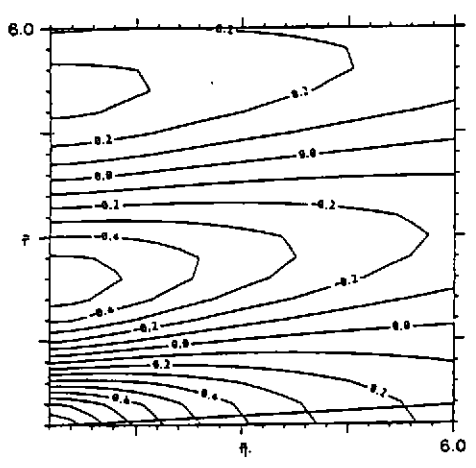


Fig. 9. A contour plot of  $F(\bar{\eta}, \bar{\tau})$ , (44) with the line  $\bar{\eta} = V\bar{\tau}$  imposed (V = 60).

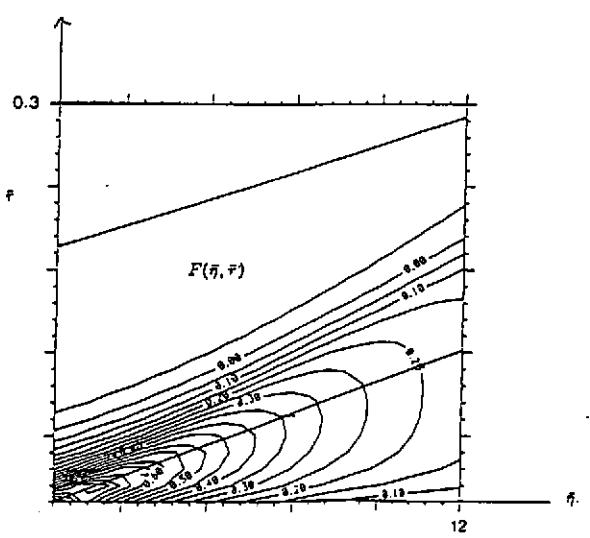


Fig. 10. A contour plot of  $F(\bar{\eta}, \bar{\tau})$ , (56), for source and receiver moving with the same parallel velocity V=64.

The line corresponding to (49) with V=60 is drawn in Figure 9. It lies very close to the  $\bar{\eta}$  axis so that the spatial effects are not much influenced by the time variation of the internal wave field itself. We see from the above that for the time dependence of internal waves to have much effect the value of V needs to be 4 or less. This implies that the receiver must move at speeds of 0.6 km/hr or less.

#### 6.2 Source and receiver in motion

In most practical situations when a towed array is used at sea, both the source and receiver will be moving. In this section we wish to study the effect that motion will have on the performances of the towed array. This will be done by finding the quantity  $F(\bar{\eta}, \bar{\tau}, V)$ , the projected integrated autocorrelation function of the medium, for the case when the source and receiver have a component of relative motion v, or V when scaled as before.

Let the velocity of the source in the y direction (i.e. transverse to the direction of propagation to the array) be  $V_S$ , that of the medium be  $V_M$  and that of the receiving array be  $V_A$ . This general formulation allows the effect of currents to be taken into account since all V can be functions of x, distance from source to receiver.

It can be shown that the normalised second moment

$$m_2(\eta, \tau, 0)/m_2(0, 0, 0)$$
 (52)

that appears in (2) for the array beam pattern is given by

$$\exp\left\{-\Gamma R[1 - F(\bar{\eta}, \bar{\tau}; V_S, V_M, V_R)]\right\}$$

$$= \exp\left\{-\Gamma R \int_0^1 [1 - f([\bar{\eta} - (V_S - V_R)\bar{\tau}]t + [V_M - V_R]\bar{\tau})]dt\right\}.$$
(53)

Here all quantities have been scaled in the usual manner, including the velocities, e.g.

$$V_S = v_S T_i / L_H$$
$$V_M = u_M T_i / L_H$$
$$V_R = v_R T_i / L_H$$

where  $v_S, v_M$  and  $v_R$  are the unscaled velocities of source, medium and receiver respectively.

The general expression

$$F(\bar{\eta}, \bar{\tau}; V_S, V_M, V_R) = \int_0^1 f([\bar{\eta} - (V_S - V_R)\bar{\tau}]t + [V_M - V_R]\bar{\tau})]dt$$
 (54)

can be derived from the time dependent form of the Garrett-Munk spectrum, but is not given here. We conclude our treatment by considering one particular case corresponding to a transmission experiment in which both source receiving array were towed by two ships steaming on parallel tracks.

6.3 The case of source moving in parallel with the receiver

Here  $V_S = V_R$ , and  $V_M = 0$  and (54) becomes

$$F(\bar{\eta},\bar{\tau}) = \int_0^1 f(\bar{\eta}t - V_R\bar{\tau})dt \tag{55}$$

which, for the internal wave standard spectrum,

$$F(\bar{\eta}, \bar{\tau}) = \frac{4}{\ln(1+j_*^2)\bar{\eta}} \int_{1/j_*}^{\infty} \frac{1}{(1+x^2)x^2} \times \int_0^{\infty} \{\sin[(\bar{\eta} - V_R \bar{\tau})xy] + \sin(V_R \bar{\tau}xy)\} \times \\ \cos(\bar{\tau} \sqrt{(1+y^2)/(1+a^2y^2)})(1+y^2)^{-2} dx dy .$$
 (56)

The function  $F(\bar{\eta}, \bar{\tau})$  is shown in Figure 10 for a particular value of  $V_R$ . As usual  $j_* = 3$  while  $v_R$  is assumed to be 9.2 km/hr. This gives

$$V_R \approx 64$$
.

Inspection of Figure 10 reveals that  $F(\bar{\eta}, \bar{\tau})$  has a maximum that lies approximately along a line

$$\bar{\eta} = V\bar{\tau} \tag{57}$$

where V has a value of about 128. This implies that the observed time-space diffraction pattern of the acoustic field has an apparent velocity

$$V = 128$$
.

This is twice the value of  $V_R$  above. The present case, where both source and receiver move at the same parallel velocity is equivalent to keeping them stationary and moving the medium with velocity  $-V_R$ . Such a case is discussed in [5] where it is shown that the apparent speed of the diffraction pattern is just twice that of the medium, giving us confidence in the present result.

#### 7. CONCLUSIONS

The relatively simple expressions derived in this paper allow the effect of internal waves on a horizontal towed array to be quickly and reliably estimated with respect to array length, angular resolution and operating frequency. Curves giving the full dependences in any particular case can easily be computed from expression (14) if required for specific design purposes.

There are, however, other effects arising from internal waves that this treatment does not address. For example, the probability of encountering a high intensity peak or a region of very low acoustic intensity and the influence of array length on this would require a rather different approach.

#### 8. ACKNOWLEDGEMENTS

This work was supported by the Commission of the European Union under Contract MAS2-CT93-0057 of the MAST-II program and by the Defence Research Agency, UK. The author was supported by the Isaac Newton Trust while writing this paper.

#### 9. REFERENCES

- [1]B.J. USCINSKI, 'Numerical simulations and moments of the field from a point source in a random medium'. J. Mod. Opt. 36, 1631-1643 (1989).
- [2] P.F. DOBBINS, 'Array directivity, sea water inhomogeneity and the plane wave spectrum', *Proc. I.O.A.* 12, Part 1, 123-130 (1990).
- [3] B.J. USCINSKI & D.E. REEVE, 'The effect of ocean inhomogeneities on array output', J. Acoust. Soc. Am. 87, 2527-2534 (1990).
- [4] W.H. MUNK & F. ZACHARIASEN, 'Sound propagation through a fluctuating stratified ocean: theory and observation', J. Acoust. Soc. Am. 59, 818-838 (1975).
- [5] B.J. USCINSKI, "The elements of wave propagation in random media", McGraw-Hill, (1977).



# The Determination of Optimum Array Lengths Based on Signal Coherence in Deep and Shallow Water

William M. Carey, ARPA, 3701 North Fairfax Dr., Arlington, Va. 22203, USA

Experimental measurements of signal coherence and array signal gain are reviewed for both deep and shallow water sound channels. The signal gain is related to single path or modal coherence lengths through well known relationships in the statistical theory of antennas. Signal gain measure-ments in the transverse and longitudinal directions are profered as the optimum measures of coherence lengths for both broadband and narrowband signals. Using this techniques measurements (<1 kHz) are presented that show for the deep water cases lengths on the order of 300 wavelengths can be achieved while in the downward refraction conditions of a shallow water waveguide lengths between 30 and 100 wavelengths are realized. The measurement of broadband and narrowband coherence and correlation functions are discussed with emphasis on the role of partly coherent noise backgrounds and multipath interference effects as well as averaging constraints. These results are interpreted with coherence models based on sound scattering from the volume and boundaries of the waveguide. The requirements for the numerical modeling of the signal coherence are presented.

Proceedings of the Institute of Acoustics